Variational selective segmentation model for intensity inhomogeneous image

Tammie Christy Saibin[1], Abdul Kadir Jumaat[2,3]
[1]School of Mathematical Sciences, College of Computing, Informatics and Media, Universiti Teknologi MARA, Kota Kinabalu, Malaysia
[2]School of Mathematical Sciences, College of Computing, Informatics and Media, Universiti Teknologi MARA, Shah Alam, Malaysia
[3]Institute for Big Data Analytics and Artificial Intelligence (IBDAAI), Universiti Teknologi MARA, Shah Alam, Malaysia

Article Info

ABSTRACT

Variational selective image segmentation models aim to extract a particular object in an image depending on a set of user-defined prior points. The current model suffers from high computational costs due to the traditional total variation function that results in a slow segmenting process. In addition, it is not designed to segment images with intensity inhomogeneities. In this research, we formulate a new variational selective image segmentation model based on the Gaussian function. A Gaussian function is proposed to replace the traditional total variation function to regularize the variational level set function. To segment images with intensity inhomogeneities, the local image fitting idea was incorporate into the formulation. The efficiency of the proposed model was then assessed by recording the computation time while the accuracy was measured using Jaccard and Dice similarity values. Numerical experiments using synthetic, natural, and medical images demonstrate that the proposed model is about 6 times faster than the existing model, while the Jaccard and Dice values are about 11% and 7% higher, respectively, compared to the existing model. In the future, this research can be extended further into a 3-dimensional modeling and vector-valued image framework.

Corresponding Author:

Abdul Kadir Jumaat
School of Mathematical Sciences, College of Computing, Informatics and Media
Institute for Big Data Analytics and Artificial Intelligence (IBDAAI), Universiti Teknologi MARA
Kompleks Al-Khawarizmi, 40450 Shah Alam, Selangor, Malaysia
Email: abdulkadir@tmsk.uitm.edu.my

1. INTRODUCTION

In order to examine and separate a digital image into different components that may be used for fundamental applications such as in the disciplines of medical diagnostics [1], and object recognition [2]–[5], image segmentation is required. Intensity inhomogeneity is one of the main obstacles to image segmentation, which is produced by errors in image acquisition, the effects of illumination, and other environmental factors. Researchers may make mistakes in interpreting an image as a result of the presence of intensity inhomogeneity in the image. As a result, segmenting an image with intensity inhomogeneity increasing the interwst of many researchers. Many approaches for image segmentation have recently been developed. The segmentation approaches can be classified into variational and non-variational segmentation approaches. Variational approaches use calculus of variations to minimize the cost energy function where the basic idea is to define an objective function and apply optimization procedures to obtain optimality (minimum or maximum), while non-variational methods are formulated based on a heuristic approach [6].

The methods of the non-variational model include region growing [7] and thresholding [8]. For a region with low contrast, noisy images, and being near to a neighboring object, region-growing and thresholding methods may give unsatisfactory results as all features or objects (including the image noise) in an image may be segmented by these two methods. Other models also utilise the machine learning-based approach. The methods used include convolutional neural networks (CNN) [9] and U-Net [10]. Studies have proven that these machine learning-based approaches to non-variational image segmentation are effective for image segmentation [11]. However, the machine learning-based approach does have its disadvantages, such as being too dependent on data and that the process of segmenting images is unknown [12].

The diverse characteristics of a set of images have been shown to be effectively handled by the variational image segmentation techniques, which also provide high-quality processing capabilities for imaging [13]-[15]. These benefits led our research to concentrate on variational image segmentation methods. An image is viewed as a function in variational image processing, with its sampling corresponding to an image's discrete matrix form. Chan and Vese [16], Zhang *et al.* [17], and Jumaat and Chen [18] introduced some examples of effective variational image segmentation models in two-dimensional formulation, while [19] formulated the three-dimensional model.

Variational image segmentation employs both global and selective segmentation techniques. The global segmentation approach refers to techniques for segmenting all objects boundaries in observed images. The famous model was developed by Chan and Vese [16]. The Chan and Vese model [16] is abbreviated as the CV model in this research. Let $z = z_0(x, y)$ be an image in domain D. In the CV model, the assumption made is that z_0 is formed by two (2) main regions, where the unknown contour γ separates the regions. Inside γ, assume the region D_1 represents the targeted object with the unknown intensity value b_1. Outside γ, the image intensity is approximated by the unknown value b_2 in $D_2 = D \backslash D_1$. Then, with $D = D_1 \cup D_2$, the CV model minimizes as shown in (1).

$$\min_{\gamma, b_1, b_2} \left\{ CV(\gamma, b_1, b_2) = \mu \text{ length } (\gamma) + \lambda_1 \int_{D_1} (z_0 - b_1)^2 \, dxdy + \lambda_2 \int_{D_2} (z_0 - b_2)^2 \, dxdy \right\} \quad (1)$$

Here, the unknown constants b_1 and b_2 are considered as the approximate piecewise constant intensities of the mean values of z_0 inside and outside the variable contour γ. The parameters μ, λ_1 and λ_2, which are non-negative parameters, represent the weights for the regularizing term and the fitting term, respectively. To evaluate in (1) in whole domain, the level set method was applied and the Heaviside function, $H(\phi(x, y)) = 0.5(1 + (2/\pi) \arctan(\phi/\varepsilon))$ and the Dirac delta function, $\delta(\phi(x, y)) = H'(\phi(x, y))$ were introduced. The function ϕ is a level set function. The contour γ is defined as the zero-level set function, i.e., $\gamma = \{(x, y) \in D | \phi(x, y) = 0\}$. The constant ε is used to avoid the values of $H(\phi(x, y))$ and $\delta(\phi(x, y))$ tends to be zero which may lead to the failure of object to be extracted if it is far from the initial contour. Thus, as in (1) is transformed into (2).

$$\min_{\phi, b_1, b_2} CV(\phi, b_1, b_2) =$$
$$\left\{ \mu \int_D |\nabla H(\phi)| \, dxdy + \lambda_1 \int_D (z_0 - b_1)^2 H(\phi) \, dxdy + \lambda_2 \int_D (z_0 - b_2)^2 (1 - H(\phi)) \, dxdy \right\} \quad (2)$$

Fixing b_1 and b_2 as constants in $CV(\phi, b_1, b_2)$ leads to in (3):

$$\mu \delta(\phi) \nabla . (\nabla \phi / |\nabla \phi|) - \lambda_1 \delta(\phi)(z_0 - b_1)^2 + \lambda_2 \delta(\phi)(z_0 - b_2)^2 = 0. \quad (3)$$

where $\nabla \phi$ represents the gradient of level set function ϕ. As shown in (3) is called the Euler Lagrange (EL) equation with Neumann boundary condition, which was solved using the gradient descent method. However, the CV model is only effective for an image with homogeneous intensity. For images with intensity inhomogeneity, this method may produce unsatisfactory results. In addition, the model is computationally complex due to the existence of the curvature term in (3) that comes from the total variation term in (2).

Consequently, Zhang *et al.* [17] proposed a global segmentation model based on local image fitting (LIF) which is capable of segmenting an image with intensity inhomogeneity. In addition, Gaussian filtering is used to regularize the level set function that results in a cheap computational cost and faster convergence. The LIF formulation is defined as (4).

$$z^{LIF} = c_1 H(\phi) + c_2 (1 - H(\phi)). \quad (4)$$

where $c_1 = \text{mean}\big(z_0 \in (\{(x,y) \in D | \phi < 0\} \cap W_k)\big)$ and $c_2 = \text{mean}\big(z_0 \in (\{(x,y) \in D | \phi < 0\} \cap W_k)\big)$. Here, $W_k(x,y)$ is a Gaussian window with standard deviation σ and size *4k+1* by *4k+1*, $k \in Z^+$. Then, the local image fitting energy function is defined as (5).

$$\min_{\phi} \left\{ E^{LIF}(\phi) = \tfrac{1}{2} \int_D (z_0 - z^{LIF})^2 \, dD \right\} \tag{5}$$

During evolution of level set function, Gaussian filtering was used to regularize the function to make the level set function smooth. By calculus of variations, the EL equation for the function in (5) is defined as $-[z_0 - c_1 H(\phi) - c_2(1 - H(\phi))](c_1 - c_2)\delta(\phi) = 0$. Using the gradient descent method, the gradient descent flow is defined as $\partial\phi/\partial t = [z_0 - c_1 H(\phi) - c_2(1 - H(\phi))](c_1 - c_2)\delta(\phi)$, used to solve the EL equation. The LIF model is suitable for global segmentation where all objects in an image will be segmented. To segment a specific object in an image, selective segmentation is more suitable. Mandal *et al.* [20] and Wei *et al.* [21] also proposed models to improve the traditional segmentation model and Chan and Vese's model [16] respectively. Rada and Chen [22] assert that global segmentation techniques cannot be used to isolate a single object in an image. In order to do this, adopting techniques for selective segmentation is a more suitable way to complete the work.

Selective segmentation is a technique of segmenting a particular object in an image based on a set of user-defined prior points called markers. With this attribute, selective segmentation has high potential to be incorporated with other computational techniques such as in medical imaging [23], [24], biometric application [25] and text processing [26]. Examples of effective models include Rada and Chen [22] and Jumaat and Chen [20]. The selective segmentation model by Jumaat and Chen [18], namely the primal dual selective segmentation (PDSS), is more effective to implement compared to Rada and Chen's model [22] as the model is convex and less sensitive to initialization. In the PDSS model, the marker set is introduced, and it is defined as $A = \{w_i = (x_i^*, y_i^*) \in D, 1 \le i \le n_1\}$ with $n_1 \ge 3$ marker points that will be placed near the targeted object. The function $P_d(x,y) = \sqrt{(x - x_p)^2 + (y - y_p)^2}$ is the Euclidean distance of each point $(x,y) \in D$ from its nearest point in the polygon, P made up of $(x_p, y_p) \in P$, constructed from the user input set, A. Then, by adjusting $H(\phi) \to u \in [0,1]$, the PDSS function is then defined as (6).

$$\min_{u,w\in[0,1]} \left\{ PDSS(u,w) = \mu \int_D |\nabla_u|_g \, dD + \int_D rw \, dD + \theta \int_D P_d w \, dD + \tfrac{1}{2\rho} \int_D (u - w)^2 \, dD \right\} \tag{6}$$

Here, $g(x,y)$ is an edge detector function, $r = (b_1 - z_0)^2 - (b_2 - z_0)^2$ is the fitting term and w is a dual variable. While this model is effective for the selective segmentation model, it may give unsatisfactory results for an image with intensity inhomogeneity due to the similar fitting term as the CV model is used in the PDSS formulation. In addition, the existence of total variation term in the formulation may increase the computational cost and results in slow convergence.

Therefore, in this research, we propose a new model by incorporating the ideas from the PDSS model [18] and Zhang *et al.* [17] into a new optimization formulation. We expected to see improvements in terms of efficiency and segmentation accuracy by modifying the PDSS model.

2. METHOD

In this section, the proposed selective segmentation model is presented. Three main ideas are incorporated in the formulation of the energy minimization function: i) A distance function which is vital to capture a specific object; ii) A local image fitting to deal with an image with intensity inhomogeneity and iii) The Gaussian function to regularize level set function. We define a marker set $A = \{w_i = (x_i^*, y_i^*) \in D, 1 \le i \le n_1\}$ with $n_1 \ge 3$ marker points that will be placed near the boundary of a targeted object in a given image $z_0(x,y)$. Then, the energy minimization function of the proposed model termed the Gaussian regularization selective segmentation (GRSS[a]) is defined as (7):

$$\min_{\phi} \left\{ GRSS^a(\phi) = \tfrac{1}{2} \int_D \big(z_0 - (f_1 H(\phi) + f_2(1 - H(\phi)))\big)^2 \, dD + \theta \int_D P_d H(\phi) \, dD \right\} \tag{7}$$

with $f_1(x,y) = k_\sigma * [H(\phi)z_0]/k_\sigma * H(\phi)$ and $f_2(x,y) = k_\sigma * [1 - H(\phi)z_0]/k_\sigma * [1 - H(\phi)]$. The function k_σ is a Gaussian kernel with standard deviation σ such that $k_\sigma = e^{-(x^2 + y^2)/2\sigma^2}$. The standard deviation σ can be viewed as a scale parameter that controls the region-scalability from a small neighbourhood to the whole image domain [27]. The function f_1 and f_2 can be interpreted as the average of image intensities in a Gaussian window inside and outside the contour respectively, defined to handle an image with intensity inhomogeneity.

The parameter θ will restrict the contour from evolving too far from the targeted object. In practice, a small θ is needed for a simple image, while a large θ is suitable for a low contrast image or an object that is close to the neighbouring area. To obtain a smooth contour, the Gaussian kernel is used to regularize the level set function after each iteration. By calculus of variation, the associated EL equation for (7) is defined as (8).

$$-\delta(\phi)\{[z_0 - f_1 H(\phi) - f_2(1 - H(\phi))](f_1 - f_2) - \theta P_d\} = 0 \tag{8}$$

As shown in (8) can be solve using the gradient descent method to obtain the following gradient descent flow:

$$\frac{\partial \phi}{\partial t} = \delta(\phi)\{[z_0 - f_1 H(\phi) - f_2(1 - H(\phi))](f_1 - f_2) - \theta P_d\} \tag{9}$$

In other word, the GRSS^a model is minimized by solving as (9).

2.1. A new variant of GRSS^a model

We also propose a new variant of the GRSS^a model, termed GRSS^b, defined as (10).

$$\min_{\phi} \left\{ GRSS^b(\phi) = \theta \int_D P_d H(\phi) dD + \int_D [(b_1 - z_0)^2 - (b_2 - z_0)^2] H(\phi) dD \right\} \tag{10}$$

The GRSS^b model uses the idea from the PDSS model. Here, the total variation term in the PDSS model is removed to reduce the complexity. To regularize the level set function, the Gaussian kernel function is adopted in the GRSS^b model. The EL equation for the GRSS^b model is $\delta(\phi)[(z_0 - b_1)^2 - (z_0 - b_2)^2 + \theta P_d] = 0$ with the following gradient descent flow as (11).

$$\frac{\partial \phi}{\partial t} = \delta(\phi)[(z_0 - b_1)^2 - (z_0 - b_2)^2 + \theta P_d] \tag{11}$$

2.2. Steps of algorithm for the proposed selective segmentation models

The following algorithms show the steps involved to implement the new proposed models; the GRSS^a model and the GRSS^b model. MATLAB R2021a software with the CPU processor of Intel® Core TM-i7-1065G7 CPU @ 1.30 GHz with 8 GB installed memory (RAM) is used in the implementation. We first demonstrate the Algorithm 1 which is the GRSS^a model. There are four steps taken, implemented in MATLAB software. The iteration process stops when the solution reaches the tolerance, *tol* or reaches the maximum iterations, *maxit*. The following is a description of the Algorithm 1:

Algorithm 1. Algorithm for GRSS^a model

1. Set the tolerance, tol , maximum iterations, *maxit*, parameters values of σ and θ and define
    the marker set A.
2. Compute and initialize the level set function ϕ.
3. **For** *iteration=1* to maximum iterations, *maxit* or $\|\phi^{n+1} - \phi^n\|/\|\phi^n\| \le tol$ **do**
Evolve the level set function ϕ based on Equation 9.
    Regularize ϕ by convolving with k_σ.
end for
4. The output ϕ will be defined as the final solution.

Next, we discuss the Algorithm 2 which is the GRSS^b model. All steps in Algorithm 2 are identical to the Algorithm 1 except in Step 2 and Step 3. In Step 2, the level set function is defined as a signed distance function while in Step 3 the evolving level set function ϕ is based on (11). The Algorithm 2 can be described as:

Algorithm 2. Algorithm for GRSS^b model

1. Set the tolerance, tol , maximum iterations, *maxit*, parameters values of σ and θ and define
    the marker set A.
2. Compute and initialize the level set function ϕ as a signed distance function.
3. **For** *iteration=1* to maximum iterations, *maxit* or $\|\phi^{n+1} - \phi^n\|/\|\phi^n\| \le tol$ **do**
Evolve the level set function ϕ based on Equation 11.
    Regularize ϕ by convolving with k_σ.
end for
4. The output ϕ will be defined as the final solution.

3. RESULTS AND DISCUSSION

In this research, the performance of the proposed selective segmentation models, GRSS[a] and GRSS[b] were compared with the existing selective segmentation model, PDSS [18]. Two similarity coefficients namely Jaccard (JSC) and Dice (DSC) were computed. A perfect segmentation quality is indicated by a value of 1 while a poor quality of segmentation is indicated by a value of 0. For all experiments, the tolerance, $tol = 10^{-6}$ and the maximum iterations, $maxit=200$. The values of σ to regularize the level set function in Algorithms 1 and 2 are in the range of $\sigma = [0.1, 0.45]$ while the values of σ to solve (9) of Algorithm 1 range from $\sigma = [5,33]$ of window size $4k+1$ by $4k+1$, $k \in Z^{+}$. The test images with their ground truth solutions are obtained from [28]-[30]. Figure 1 demonstrates the segmentation results of all models in segmenting natural images. The first and fifth columns show the natural test images with the marker set in green. The second and sixth columns demonstrate the results for GRSS[a] model. The results for GRSS[b] model are indicated in the third and seventh columns while the fourth and the last column show the results for the PDSS model. The values of θ range from $\theta = [150, 2000]$.
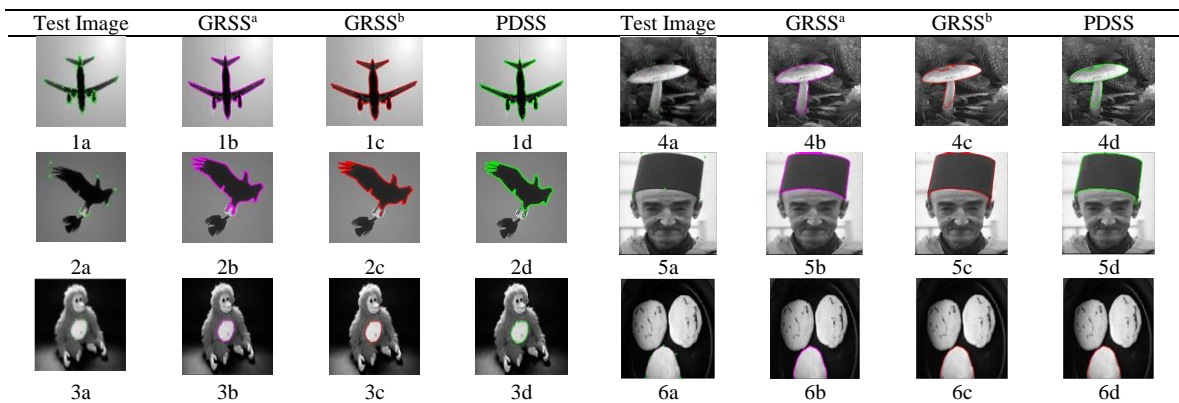
Test Image	GRSS[a]	GRSS[b]	PDSS	Test Image	GRSS[a]	GRSS[b]	PDSS
1a	1b	1c	1d	4a	4b	4c	4d
2a	2b	2c	2d	5a	5b	5c	5d
3a	3b	3c	3d	6a	6b	6c	6d

Figure 1. Segmentation results on natural images

By visual observation, all models successfully segmented the targeted object. However, our GRSS[a] model gave more accurate results, especially in segmenting the big bird in Figure 1(2b) and the mushroom in Figure 1(4b). Table 1 shows the computation time, JSC and DSC values of each model for each natural image.

Table 1. The computation time, JSC and DSC values for each model in segmenting natural images

Test Image	1a	2a	3a	4a	5a	6a
GRSS[a] Time/JSC/DSC	1.03/0.89/0.94	0.93/0.90/0.95	1.87/0.92/0.96	7.38/0.94/0.97	2.13/0.93/0.96	1.34/0.90/0.95
GRSS[b] Time/JSC/DSC	1.68/0.90/0.95	3.96/0.87/0.93	0.61/0.92/0.96	1.10/0.87/0.93	0.74/0.92/0.96	0.73/0.88/0.94
PDSS Time/JSC/DSC	37.83/0.89/0.94	30.43/0.87/0.93	7.14/0.92/0.96	6.72/0.86/0.92	10.23/0.92/0.96	10.39/0.88/0.94

Besides qualitative analysis by visual observation, we also provide a quantitative analysis of the segmentation accuracy by evaluating JSC and DSC values as well as the computation time as indicated in Table 1. For all tested images, the computation times for our proposed GRSS[a] and GRSS[b] are faster than PDSS. This is due to the advantage of using Gaussian kernel to regularize the level set function which is more efficient compared to the total variation regularization term. For an image with high intensity inhomogeneity in test images 2a, 4a and 6a, the GRSS[a] model had higher JSC and DSC values compared to the other models. For test image 1a, the model GRSS[b] had slightly higher values of JSC and DSC than the GRSS[a] and PDSS models. Besides natural images, we also tested all models in segmenting medical images as demonstrated in Figure 2.

The values of θ used range from $\theta = [655, 5000]$. Figure 2(7a) is an x-ray hand image, Figure 2(8a) and (9a) are blood vessel images, Figure 2(10a-13a) are breast ultrasound images, while Figure 2(14a) is skin abnormality image. The qualitative analysis (by visual evaluation) indicates that the GRSS[a] model gave more accurate results. For quantitative analysis, we tabulated the computing time, JSC and DSC values for all models in segmenting the medical images in Table 2.

The data in Table 2 confirms that the GRSS[a] model is more accurate compared to GRSS[b] and PDSS as indicated by the JSC and DSC values except for test image 14a where the segmentation accuracy for all models are similar. In terms of computation time, the GRSS[a] model is faster than the other two models for test images 7a and 11a while for other test images, the GRSS[b] model is faster than GRSS[a] and PDSS models. To complete the experiment, we demonstrate the segmentation of all models in segmenting synthetic images as shown in Figure 3. The values of the θ used range from $\theta = [15,1300]$.
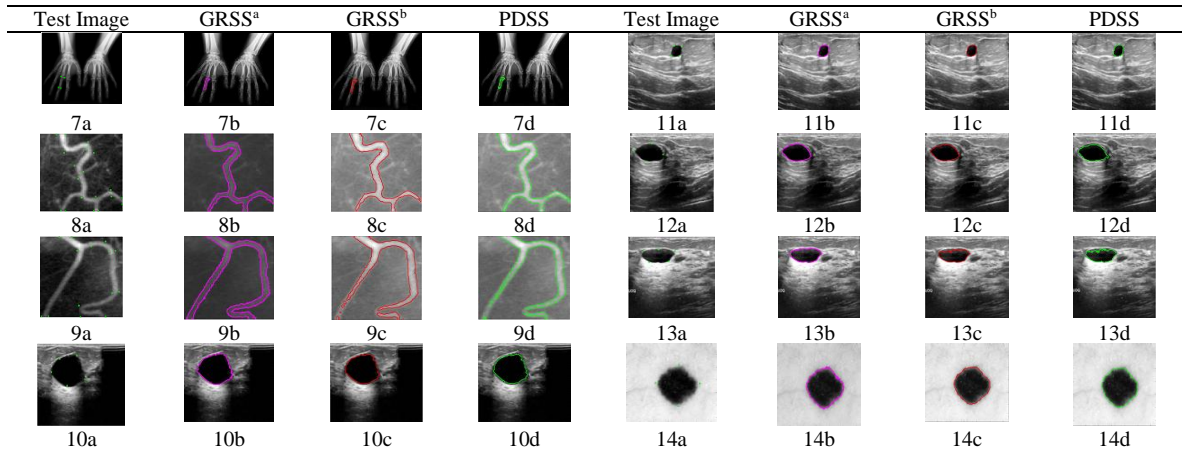
Figure 2. Segmentation results on medical images

Table 2. The computation time, JSC and DSC values for each model in segmenting medical image

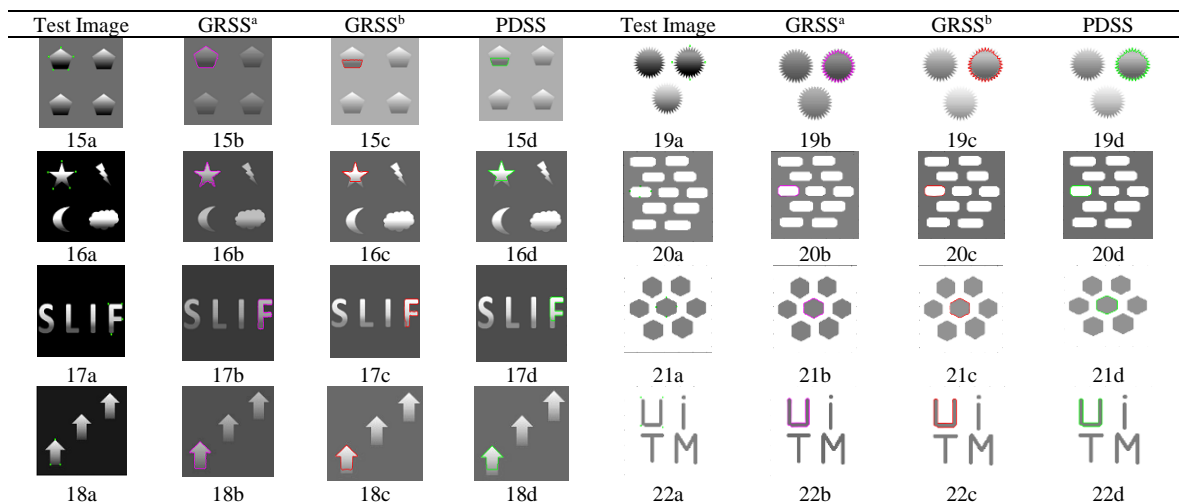| Test Image	7a	8a	9a	10a	11a	12a	13a	14a
GRSS[a] Time/JSC/DSC	0.62/0.81/ 0.90	9.39/0.90/ 0.95	8.19/0.90/ 0.95	2.20/0.94/ 0.97	0.45/0.91/ 0.95	1.35/0.90 / 0.95	1.13/0.92/ 0.96	3.63/0.8 0/0.89
GRSS[b] Time/JSC/DSC	3.02/0.79/ 0.88	1.76/0.77/ 0.87	1.99/0.72/0. 84	0.73/0.89/0. 94	0.60/0.85/ 0.92	0.63/0.84 / 0.91	0.82/0.80/ 0.89	1.00/0.8 0/0.89
PDSS Time/JSC/DSC	54.16/0.7 3/ 0.84	12.42/0.7 8/ 0.88	17.76/0.7/ 0.82	8.46/0.88/ 0.94	9.85/0.85/ 0.92	16.85/0.8 5/0.92	15.09/0.79/0 .88	9.63/0.8 0/0.89

Figure 3. Segmentation results on synthetic images

By visual inspection, the GRSS[a] model is more accurate compared to GRSS[b] and PDSS. Thanks to the local fitting term that gives advantage to the proposed GRSS[a] model in segmenting the synthetic images with intensity inhomogeneity, for test images 15a-19a the GRSS[b] and PDSS models struggled to segment the inhomogeneous intensity image. This shows that the average intensity fitting term in their formulation is insufficient to segment this kind of image. To further investigate, the data on the computing time, JSC and DSC values are recorded and tabulated in Table 3.

Table 3. The computation time, JSC and DSC values for each model in segmenting synthetic images

Test Image	15a	16a	17a	18a	19a	20a	21a	22a
GRSS[a] Time/JSC/DSC	0.86/0.95/ 0.97	2.51/0.84 /0.92	1.69/0.88/0. 93	2.95/0.94/0. 97	6.98/0.87/0. 93	0.61/1.0/ 1.0	0.59/1.0/ 1.0	0.74/1. 0/1.0
GRSS[b] Time/JSC/DSC	1.45/0.37/ 0.54	1.05/0.73/ 0.84	0.69/0.84/0. 91	0.76/0.79/0. 88	0.72/0.85/0. 92	0.69/1.0/ 1.0	0.74/1.0/ 1.0	0.79/1. 0/1.0
PDSS Time/JSC/DSC	11.99/0.37/0 .54	7.75/0.72/0 .84	11.97/0.73/0 .84	11.95/0.72/ 0.84	10.63/0.84/ 0.91	6.60/1.0/ 1.0	6.52/0.995/0. 998	9.79/1. 0/ 1.0

Based on Table 3, it is confirmed that the GRSS[a] model is more accurate compared to GRSS[b] and PDSS in segmenting synthetic images with intensity inhomogeneity which are images 15a-19a. For homogeneous synthetic test images (images 20a-22a), a perfect score of JSC and DSC values were obtained by all models except for the the PDSS model in segmenting test image 21a. For test images 15a, 20a-22a, the computation time for the GRSS[a] model was faster than GRSS[b] and PDSS while the GRSS[b] model was faster than other models in segmenting the remaining synthetic images. The slowest computing time was delivered by the PDSS model. Again, this is the evidence of the advantage of using Gaussian function to regularize the level set function in our GRSS[a] and GRSS[b] models.

Based on Table 1, 2 and 3, for all 22 test images used, the average of computing times for GRSS[a], GRSS[b] and PDSS model are 2.66s, 1.19s and 14.73s respectively. The average values of JSC for GRSS[a], GRSS[b] and PDSS model are 0.91, 0.84 and 0.82 respectively while the average values of DSC for GRSS[a], GRSS[b] and PDSS model are 0.95, 0.90 and 0.89 respectively. These data demonstrate that GRSS[b] is about 2 times faster than GRSS[a] and 12 times faster than PDSS model, while GRSS[a] model is 6 times faster than PDSS model. The highest values of JSC and DSC are given by GRSS[a] model which are about 9% and 5% higher than GRSS[b] respectively, while comparison between GRSS[a] model with PDSS shows that the JSC and DSC values for GRSS[a] are about 11% and 7% higher than PDSS respectively.

4. CONCLUSION

The selective segmentation method was utilized in this study to selectively segment a certain object in grayscale digital images. This study has presented two new models, termed GRSS[a] and GRSS[b]. The corresponding Euler Lagrange equations for each model were provided to minimize the functions. The equations were then solved in the MATLAB platform using the gradient descent algorithm. By analyzing the execution time and accuracy of segmentation results quantified in terms of JSC and DSC for each test image, the performance of each model was assessed both visually and numerically. The existing model, PDSS, on average, was slower than the GRSS[a] and GRSS[b] models. On the contrary, in average GRSS[b] performed faster than GRSS[a] model. Improvement in computing time was achieved in GRSS[a] and GRSS[b] models due to the application of Gaussian kernel to regularize the level set function instead of the famous total variation term. By visual observation, all models were able to segment a targeted object in each test image. High segmentation accuracy was delivered by the GRSS[a] model especially for images with intensity inhomogeneity. This observation was proven numerically by the values of JSC and DSC where the GRSS[a] model scored higher accuracy compared to the GRSS[b] and PDSS models. This achievement was due to the advantage of incorporating a local image information that fits in the GRSS[a] model that can help in segmenting an image with intensity inhomogeneity. In conclusion, the GRSS[a] model is more recommended due to its ability to handle image with intensity inhomogeneity. In future, the GRSS[a] model will be extended to colour images and 3-dimensional images since the colour and 3-dimensional images have more information.

ACKNOWLEDGEMENTS

REFERENCES

[1]   S. N. Kumar, A. L. Fred, H. A. Kumar, and P. S. Varghese, "Performance metric evaluation of segmentation algorithms for gold standard medical images," in *Advances in Intelligent Systems and Computing*, vol. 709, 2018, pp. 457–469.

[2]   S. S. Yasiran *et al.*, "Comparison between GVF snake and ED snake in segmenting microcalcifications," in *ICCAIE 2011 - 2011 IEEE Conference on Computer Applications and Industrial Electronics*, Dec. 2011, pp. 597–601, doi: 10.1109/ICCAIE.2011.6162204.

[3]   A. K. Jumaat, W. E. Rahman, A. Ibrahim, S. S. Yasiran, R. Mahmud, and A. A. Malek, "Masses characterization based on angular margin measurement," in *Proceedings of International Conference on Computational Intelligence, Modelling and Simulation*, Sep. 2012, pp. 265–269, doi: 10.1109/CIMSim.2012.50.

[4]   S. S. Yasiran *et al.*, "Microcalcifications segmentation using three edge detection techniques," in *International Conference on Electronic Devices, Systems, and Applications*, Nov. 2012, pp. 207–211, doi: 10.1109/ICEDSA.2012.6507798.

[5]   A. K. Jumaat *et al.*, "Performance comparison of Canny and Sobel edge detectors on Balloon Snake in segmenting masses," in *2014 International Conference on Computer and Information Sciences, ICCOINS 2014 - A Conference of World Engineering, Science and Technology Congress, ESTCON 2014 - Proceedings*, Jun. 2014, pp. 1–5, doi: 10.1109/ICCOINS.2014.6868368.

[6]   A. B. Yearwood, "A brief survey on variational methods for image segmentation," *Research Assignment: Chicago Referencing*, no. March, pp. 1–7, 2018.

[7]   X. Jiang, Y. Guo, H. Chen, Y. Zhang, and Y. Lu, "An Adaptive Region Growing Based on Neutrosophic Set in Ultrasound Domain for Image Segmentation," *IEEE Access*, vol. 7, pp. 60584–60593, 2019, doi: 10.1109/ACCESS.2019.2911560.

[8]   R. I. R. Thanaraj, B. Anand, J. A. Rahul, and V. Rajinikanth, "Appraisal of Breast Ultrasound Image Using Shannon's Thresholding and Level-Set Segmentation," 2020, pp. 621–630.

[9]   W. K. Moon, Y. W. Lee, H. H. Ke, S. H. Lee, C. S. Huang, and R. F. Chang, "Computer-aided diagnosis of breast ultrasound images using ensemble learning from convolutional neural networks," *Computer Methods and Programs in Biomedicine*, vol. 190, p. 105361, Jul. 2020, doi: 10.1016/j.cmpb.2020.105361.

[10]   M. Amiri, R. Brooks, B. Behboodi, and H. Rivaz, "Two-stage ultrasound image segmentation using U-Net and test time augmentation," *International Journal of Computer Assisted Radiology and Surgery*, vol. 15, no. 6, pp. 981–988, Jun. 2020, doi: 10.1007/s11548-020-02158-3.

[11]   S. Masood, M. Sharif, A. Masood, M. Yasmin, and M. Raza, "A Survey on Medical Image Segmentation," *Current Medical Imaging Reviews*, vol. 11, no. 1, pp. 3–14, Apr. 2015, doi: 10.2174/1573405611101150423103441.

[12]   L. K. Lee, S. C. Liew, and W. J. Thong, "A review of image segmentation methodologies in medical image," in *Lecture Notes in Electrical Engineering*, vol. 315, 2015, pp. 1069–1080.

[13]   K. Dilpreet and K. Yadwinder, "Various Image Segmentation Techniques: A Review," *International Journal of Computer Science and Mobile Computing*, vol. 3, no. 5, pp. 809–814, 2014.

[14]   M. W. Khan, "A Survey: Image Segmentation Techniques," *International Journal of Future Computer and Communication*, pp. 89–93, 2014, doi: 10.7763/ijfcc.2014.v3.274.

[15]   A. K. Jumaat and K. Chen, "An optimization-based multilevel algorithm for variational image segmentation models," *Electronic Transactions on Numerical Analysis*, vol. 46, pp. 474–504, 2017.

[16]   T. F. Chan and L. A. Vese, "Active contours without edges," *IEEE Transactions on Image Processing*, vol. 10, no. 2, pp. 266–277, 2001, doi: 10.1109/83.902291.

[17]   K. Zhang, H. Song, and L. Zhang, "Active contours driven by local image fitting energy," *Pattern Recognition*, vol. 43, no. 4, pp. 1199–1206, Apr. 2010, doi: 10.1016/j.patcog.2009.10.010.

[18]   A. K. Jumaat and K. Chen, "A reformulated convex and selective variational image segmentation model and its fast multilevel algorithm," *Numerical Mathematics*, vol. 12, no. 2, pp. 403–437, Jun. 2019, doi: 10.4208/nmtma.OA-2017-0143.

[19]   A. K. Jumaat and K. Chen, "Three-Dimensional Convex and Selective Variational Image Segmentation Model," *Malaysian Journal of Mathematical Sciences*, vol. 14, no. 3, pp. 437–450, 2020.

[20]   S. Mandal, X. L. Dean-Ben, and D. Razansky, "Visual quality enhancement in optoacoustic tomography using active contour segmentation priors," *IEEE Transactions on Medical Imaging*, vol. 35, no. 10, pp. 2209–2217, Oct. 2016, doi: 10.1109/TMI.2016.2553156.

[21]   W. B. Wei, L. Tan, M. Q. Jia, and Z. K. Pan, "Normal vector projection method used for convex optimization of chan-vese model for image segmentation," *Journal of Physics: Conference Series*, vol. 787, no. 1, 2017, doi: 10.1088/1742-6596/787/1/012016.

[22]   L. Rada and K. Chen, "Improved selective segmentation model using one level-set," *Journal of Algorithms and Computational Technology*, vol. 7, no. 4, pp. 509–540, 2013, doi: 10.1260/1748-3018.7.4.509.

[23]   N. F. Idris, M. A. Ismail, M. S. Mohamad, S. Kasim, Z. Zakaria, and T. Sutikno, "Breast cancer disease classification using fuzzy-ID3 algorithm based on association function," *IAES International Journal of Artificial Intelligence (IJ-AI)*, vol. 11, no. 2, p. 448, Jun. 2022, doi: 10.11591/ijai.v11.i2.pp448-461.

[24]   H. M. Ahmed and M. Y. Kashmola, "A proposed architecture for convolutional neural networks to detect skin cancers," *IAES International Journal of Artificial Intelligence (IJ-AI)*, vol. 11, no. 2, p. 485, Jun. 2022, doi: 10.11591/ijai.v11.i2.pp485-493.

[25]   A. H. T. Al-Ghrairi, A. A. Mohammed, and E. Z. Sameen, "Face detection and recognition with 180 degree rotation based on principal component analysis algorithm," *IAES International Journal of Artificial Intelligence*, vol. 11, no. 2, pp. 593–602, 2022, doi: 10.11591/ijai.v11.i2.pp593-602.

[26]   M. Z. Ansari, T. Ahmad, M. M. S. Beg, and N. Bari, "Language lexicons for Hindi-English multilingual text processing," *IAES International Journal of Artificial Intelligence (IJ-AI)*, vol. 11, no. 2, p. 641, Jun. 2022, doi: 10.11591/ijai.v11.i2.pp641-648.

[27]   L. Chunming, K. Chiu-Yen, Gore John C, and D. Zhaohua, "Minimization of region-scalable fitting energy for image segmentation," *IEEE Transactions on Image Processing*, vol. 17, no. 10, pp. 1940–1949, 2008.

[28]   T. Dietenbeck, M. Alessandrini, D. Friboulet, and O. Bernard, "Creaseg: A free software for the evaluation of image segmentation algorithms based on level-set," *Proceedings - International Conference on Image Processing, ICIP*, pp. 665–668, 2010, doi: 10.1109/ICIP.2010.5652991.

[29]   A. Rodtook, K. Kirimasthong, W. Lohitvisate, and S. S. Makhanov, "Automatic initialization of active contours and level set method in ultrasound images of breast abnormalities," *Pattern Recognition*, vol. 79, pp. 172–182, Jul. 2018, doi: 10.1016/j.patcog.2018.01.032.

[30]   N. C. F. Codella *et al.*, "Skin lesion analysis toward melanoma detection: A challenge at the 2017 International symposium on biomedical imaging (ISBI), hosted by the international skin imaging collaboration (ISIC)," in *Proceedings - International Symposium on Biomedical Imaging*, Apr. 2018, vol. 2018-April, pp. 168–172, doi: 10.1109/ISBI.2018.8363547.

BIOGRAPHIES OF AUTHORS

Tammie Christy Saibin received her B.Sc degree in Mathematics from Universiti Teknologi MARA (UiTM) Shah Alam and M.Sc degree in Universiti Kebangsaan Malaysia. She is now serving as a senior lecturer at the Faculty of Computer & Mathematical Sciences. Her research interests include image processing and fuzzy medical images. She can be contacted at email: tammi023@uitm.edu.my.

Abdul Kadir Jumaat received the B.Sc. and M.Sc. degrees in Mathematics from the Universiti Teknologi MARA, (UiTM) Shah Alam, Malaysia and the Ph.D. degree in Applied Mathematics (Mathematical Imaging Methods) from the University of Liverpool, United Kingdom. He is now serving as a senior lecturer at the Faculty of Computer and Mathematical Sciences and a research fellow at the Institute for Big Data Analytics and Artificial Intelligence (IBDAAI) in UiTM Shah Alam, Malaysia. His research interests include image/signal processing, artificial intelligence, computer vision, biometrics, medical image and analysis, and pattern recognition. He can be contacted at email: abdulkadir@tmsk.uitm.edu.my.